AIP | The Journal of Chemical Physics

Formation mechanism for polycyclic aromatic hydrocarbons in methane flames

K. Siegmann and K. Sattler

Citation: The Journal of Chemical Physics **112**, 698 (2000); doi: 10.1063/1.480648
View online: http://dx.doi.org/10.1063/1.480648
View Table of Contents: http://scitation.aip.org/content/aip/journal/jcp/112/2?ver=pdfcov
Published by the AIP Publishing

Formation mechanism for polycyclic aromatic hydrocarbons in methane flames

K. Siegmann[a)]
*Swiss Federal Institute of Technology (*ETH*), Laboratory for Solid State Physics, CH-8093 Zurich, Switzerland*

K. Sattler
University of Hawaii, Department of Physics and Astronomy, 2505 Correa Road, Honolulu, Hawaii 96822

(Received 24 August 1999; accepted 13 October 1999)

A laminar diffusion flame of methane was investigated using time-of-flight mass spectroscopy with two-photon UV laser ionization. Benzenoid polycyclic aromatic hydrocarbons (PAHs) up to 788 amu ($C_{64}H_{20}$) were detected in the combustion gases. Only the most compact PAHs are formed in the flame. The observed groups of PAH peaks with 24 amu spacings belong to PAHs with constant hydrogen content and are separated by 26 amu gaps. The sequences of PAH peaks with 24 amu spacing are explained by a repetitive bay closure mechanism. The first PAH of a constant H-sequence is proposed to form by a dimerization process. The PAHs observed can be arranged in a repetitive pattern in Dias's formula periodic system. © *2000 American Institute of Physics.* [S0021-9606(00)00902-8]

I. INTRODUCTION

Polycyclic aromatic hydrocarbons (PAHs) are in our air environment[1–3] in the form of volatile and particulate pollutants[4–6] as a result of incomplete combustion. A number of different sources cause PAH emissions: diesel and gasoline exhausts,[7–17] coal-fired, electricity generating power plants,[18,19] tobacco smoke,[20] residential wood or coal combustion,[21–24] burning of plastics,[25] and area sources such as forest fires and agricultural burning.

Formation of PAHs in flames has been studied both experimentally and theoretically by a number of groups.[26–36] Kinetic and thermodynamic modeling[34,37] and molecular orbital treatment[38] have been performed to understand the mechanisms of fused aromatic hydrocarbon formation. Methods such as mass spectroscopy,[39–42] chromatography,[43] infrared analysis,[44,45] or photoelectric charging[46] were applied. Also, the PAH formation in the universe[47,48] has been studied. The technologically important soot formation in combustion processes has been related to PAH precursors.[49–51] The most often studied environments for PAH growth in combustion were methane,[26,27,31,40,41,52–54] acetylene,[29,30,55] ethylene,[30,56] ethene,[42] propane,[57,58] butane,[59] ethane,[31,53,60] and other aliphatic[61] flames.

Methane is used as fuel in many applications including heating systems and gas turbines for electric power generation.[62–64] The combustion of natural gas (methane) is a clean and efficient process. While gas turbines operating with methane are primarily used in electric power plants, many other applications including aircraft, rail locomotives, and ships are possible. Because of its high hydrogen content, methane combustion leads to less environmental pollution than other hydrocarbon fuels. Therefore, gas turbines powered by methane are promising for future applications, which guarantee clean air conditions. Also, the replacement of alkane fuels by methane would somewhat reduce the carbon dioxide emission and the greenhouse effect.

Even though methane is a fuel with little particulate and gaseous emissions, these species are produced in the interior of the flame. The yellow color shows the presence of soot particles in the flame as they radiate due to Planck's law. The major molecular hydrocarbon species in the flame are PAHs. Both PAHs and soot particles are produced in high abundance within the flame, but are not released to the environment. PAH growth is generally considered to be governed by acetylene addition, but a detailed analysis of the PAH fingerprints in flames has not been given. The methane flame is the most basic system to study PAHs. For alkane fuels the decomposition of the molecule may lead to more complicated processes in PAH growth compared with that for methane. Therefore, the interior of the methane flame is a model system to study the basics of PAH formation.

In this paper, we give the PAH distribution sampled by mass spectrometry from a laminar methane diffusion flame. We show that a large number of different PAHs are extracted from the flame with masses up to 788 amu ($C_{64}H_{20}$). We discuss the many possible PAHs in this size range and give some of their properties. We show that the methane flame does not contain all the energetically stable PAHs but only a very small fraction of these. It turns out that only the compact PAHs are formed in the flame while the other PAHs are not. This is a puzzling result as the less-compact PAHs are stable enough to exist in the flame.

From the hydrogen content of the observed PAHs, information about their structure can be obtained. In our measurements, the predominant mass peaks are the ones of the even-numbered PAHs. This result is obtained from the analysis of neutral molecules. When charged molecules are detected,

[a)]Author to whom correspondence should be addressed. Electronic mail: K.siegmann@solid.phys.ethz.ch

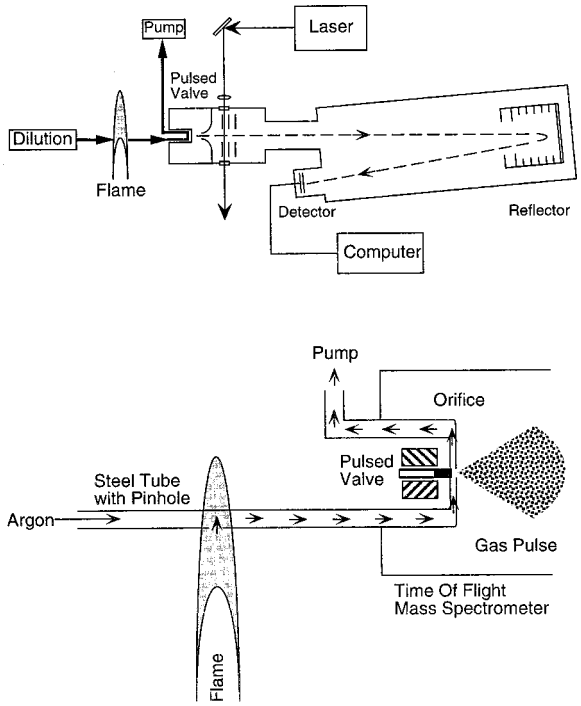

FIG. 1. Experimental setup showing flame, inlet system, and mass spectrometer. Below, the inlet system is drawn enlarged.

odd-numbered PAHs have a higher concentration.[55] Besides all-hexagon PAHs, cyclo-penta fused PAHs, containing pentagons in the otherwise hexagonal network, were also found in flames.[56,65] The mass spectra from laminar methane diffusion flames are dominated by even-numbered PAHs and therefore we will concentrate on these species.

II. EXPERIMENT

A laminar, atmospheric pressure diffusion flame burning with argon diluted methane (CH_4) is investigated.[41] Gas probes from the flame are analyzed by time-of-flight mass spectroscopy (TOF-MS) combined with UV-laser ionization. Figure 1 shows the experimental setup. Above, the flame and the TOF-MS (commercially available from Bruker-Franzen, Inc.) are displayed. Below, the extraction unit of gas probes and the inlet system for the TOF-MS are shown. A pinhole (1-mm diameter) in a steel tube is placed in the centerline of the flame. A slight underpressure is applied to continuously extract combustion gases. The gases are immediately diluted with argon at room temperature, quenching all reactions. The diluted combustion gases are guided past an orifice (0.4-mm diameter) equipped with a pulsed valve. The valve opens for about 1 ms, forming a supersonic gas jet in the high-vacuum chamber of the TOF-MS. PAHs in the gas pulse are ionized by a light pulse from an excimer laser at a wavelength of 248 nm and a duration of 20 ns. The positive ions are accelerated by high voltage. Their flight times in the drift tube are determined and their masses are calculated. Several thousand spectra are accumulated in order to increase sensitivity. It was shown previously that the sampling system produces no artifacts[66,67] and it was used in earlier studies for PAH and soot particle formation in flames.[41,68–72]

III. RESULTS AND DISCUSSION

Figure 2 gives a mass spectrum in the range where the PAHs with the smallest masses appear. The first major hydrocarbon peaks are at 78, 128, 178, and 202 amu, corresponding to C_6H_6, $C_{10}H_8$, $C_{14}H_{10}$, and $C_{16}H_{10}$, respectively. The peak of benzene (C_6H_6) is followed by the peaks of naphthalene ($C_{10}H_8$), anthracene, and phenanthrene ($C_{14}H_{10}$), and pyrene ($C_{16}H_{10}$) with one, two, three, and four hexagonal carbon rings, respectively. The peaks at C_6H_6 and $C_{10}H_8$ are entirely due to benzene and naphthalene, respectively, as these molecules have no benzenoid isomers. Anthracene and phenanthrene have the same mass but different

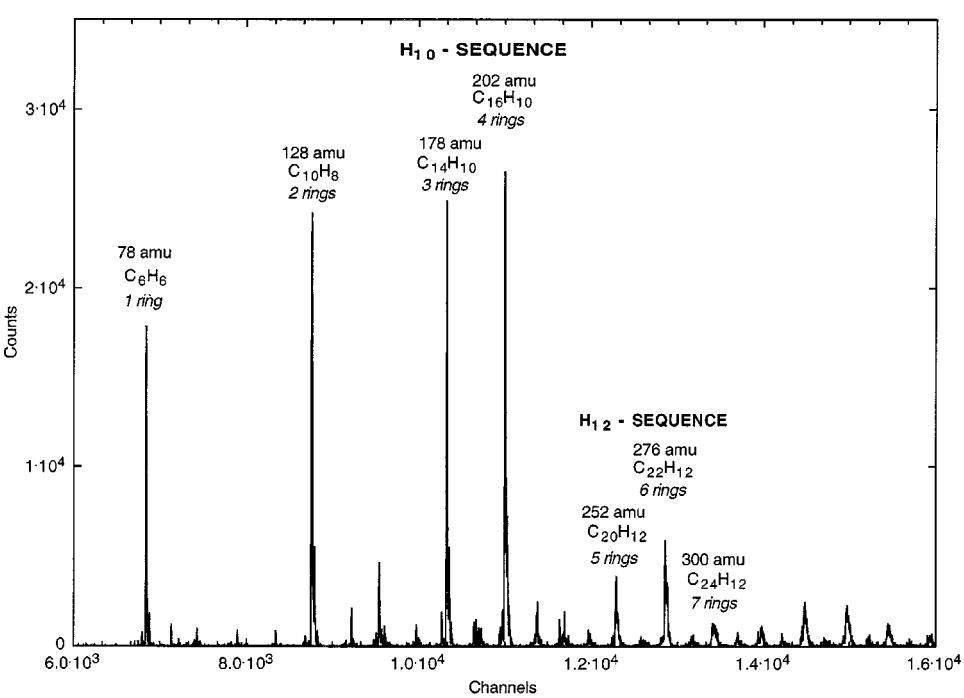

FIG. 2. Section of the mass spectrum. The first seven major peaks are labeled.

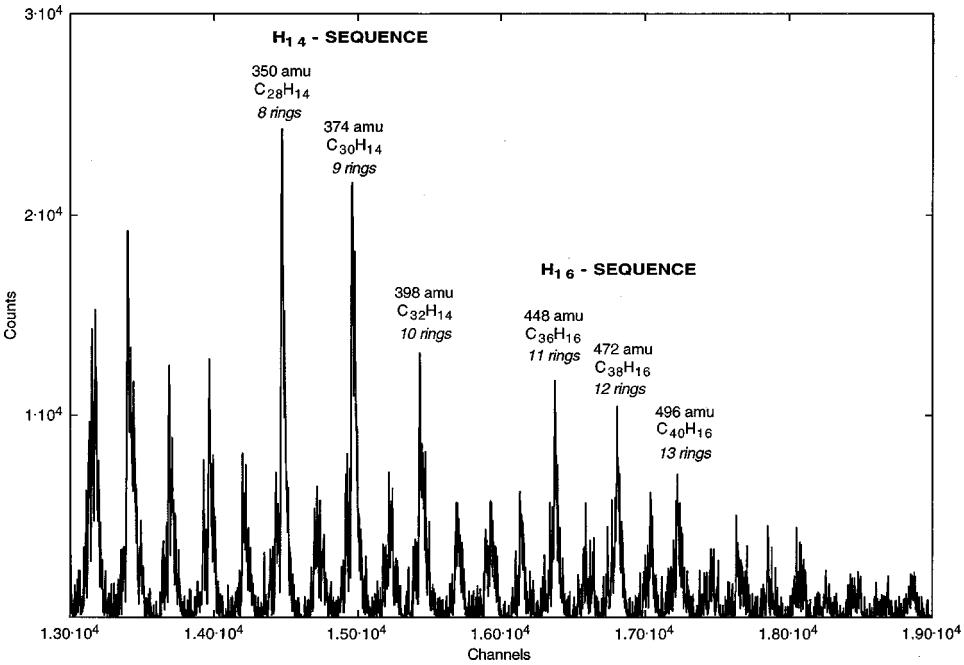

FIG. 3. Section of the mass spectrum, showing the H_{14}- and H_{16}-sequences.

geometry. In anthracene the hexagons are arranged in a straight line, while they are arranged along a kinked line in phenanthrene.

It appears to be convenient (as described in detail later) to arrange the PAH peaks in sequences with constant number of H atoms. The first such series is the one with 10 hydrogen atoms; $C_{14}H_{10}$ and $C_{16}H_{10}$. Then, the H_{12} sequence follows with three members, $C_{20}H_{12}$, $C_{22}H_{12}$, and $C_{24}H_{12}$. Between the major PAH peaks there are smaller peaks in the mass spectrum which correspond to nonbenzenoid PAHs. Since these PAHs contain odd numbers of C atoms, they cannot be completely conjugated. They are generally less stable than molecules of comparable structure containing even numbers of C atoms. Therefore, we only discuss the most abundant PAHs, which are the even-numbered PAHs.

The number of rings N_r in a benzenoid PAH can be calculated by the formula $N_r=\{(N_C-N_H)/2\}+1$, where N_C and N_H are the numbers of carbon and hydrogen atoms, respectively. This formula is valid for all isomers having the same molecular formula. In Fig. 2 we give the mass, molecular formula, and number of rings for each prominent mass peak. We see that the major mass peaks are due to the benzenoid PAHs. Starting with benzene, with one ring, the observed PAHs have 2, 3, 4, 5, etc. rings; i.e., by repeated addition of one ring we obtain all the prominent PAH peaks.

Figure 3 shows the prominent mass peaks between 350 and 496 amu. We find that there are two distinct sequences of peaks. The first sequence consists of PAHs with 14 hydrogen atoms each: $C_{28}H_{14}$, $C_{30}H_{14}$, and $C_{32}H_{14}$, and the second set with 16 hydrogen atoms each; $C_{36}H_{16}$, $C_{38}H_{16}$, and $C_{40}H_{16}$. Within one sequence the difference between two peaks is 24 amu; then there is a 26 amu difference at the transition to the next sequence. This new sequence again has 24 amu peak spacing. It follows that within one sequence the number of carbon atoms increases by 2, but there is a major interruption of this behavior from sequence to sequence. In Fig. 3 we again give the number of rings for the PAH structures of each peak. The prominent peaks are the ones with 8, 9, 10, etc. rings. Again, one ring after the other is added to the PAHs. This is given within a sequence where the peak distance is 24 amu, but also between two sequences where the PAH peak distance is 50 amu (=24+26 amu).

The overall shape of the PAH peak distribution is an exponentially decreasing curve. However, we see from Fig. 3 that the curve is not at all smooth. Whenever a new constant-hydrogen sequence starts, the intensity of the first member is much higher than the one of its predecessors.

In Fig. 4 we show the mass spectrum of the H_{16}-sequence taken at higher counting statistics, with prominent peaks at 448, 472, 496, and 520 amu. In order to assign the peaks to the corresponding PAHs, we have indicated with Lorentz curves the locations of PAHs as given by the mass calibration of the TOF instrument. We see that the mass peaks fall together exactly with the sequence $C_{36+2n}H_{16}$ in this size range.

The next set of prominent peaks starts at 546 amu with the H_{18}-sequence. The mass spectrum of Fig. 5 shows a sequence of PAH peaks $C_{44+2n}H_{18}$, again keeping the number of H atoms constant within the set. The number of carbon rings ranges from 14 to 18, with each subsequent mass peak having one additional ring.

The next series of peaks is the H_{20}-sequence, shown in Fig. 6. It gives a series of peaks $C_{52+2n}H_{20}$ for PAHs with 20 hydrogen atoms each and differing by C_2, in the range from 644 to 788 amu. The 788 amu peak is the last one which could be identified above the noise level.

Summarizing the analysis of Figs. 2–6 we find that the mass spectra consist of well-separated and characterized sequences of prominent peaks for PAHs with even numbers of carbon and hydrogen atoms. Within one sequence the number of hydrogen atoms is the same, while the number of carbon atoms increases by 2. This leads to a distance be-

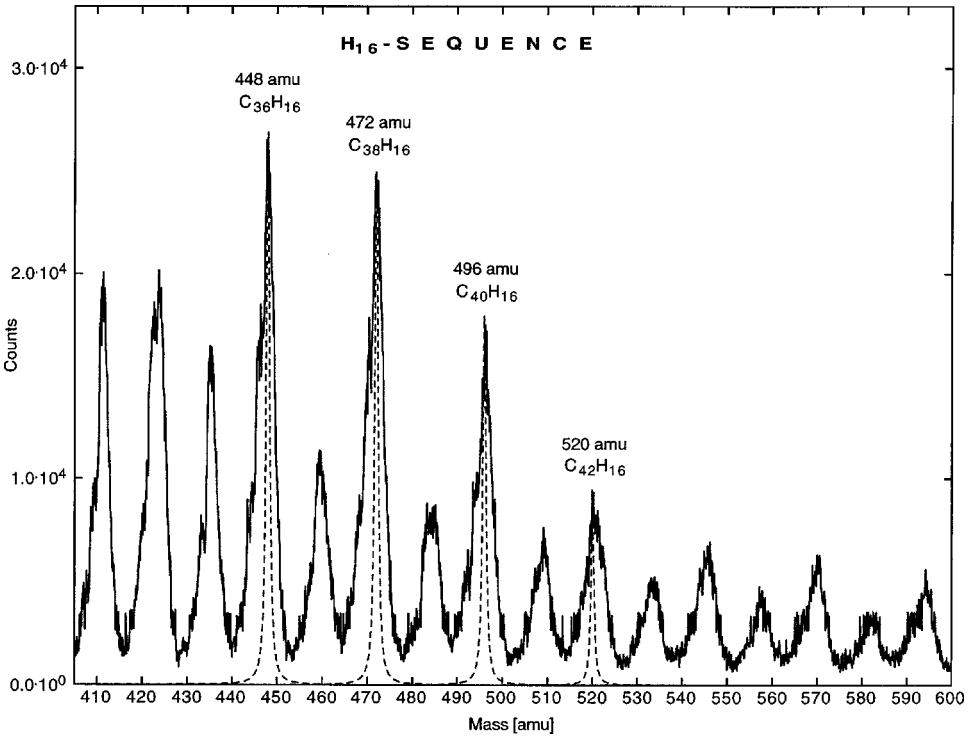

FIG. 4. Section of the mass spectrum, showing the H_{16}-sequence together with Lorentz calibration curves.

tween the peaks in one sequence by 24 amu. Then, from one set to another, this sequence is broken as there is a change in mass by 26 amu.

In Fig. 7 we zoom into a small region of the mass spectrum of Fig. 3 and analyze the peaks at 350, 374, and 398 amu. These three peaks constitute the H_{14}-sequence. They correspond to the PAHs with the formulas $C_{28}H_{14}$, $C_{30}H_{14}$, and $C_{32}H_{14}$. The dotted lines are Lorentz curves with height and width chosen to coincide with the measured mass peaks. The Lorentz curves indicate the expected positions of these peaks corresponding to the calibrated mass scale of the instrument. In addition, we plot the mass peaks expected for PAHs with higher hydrogen contents. There are two possible $C_{28}H_x$ PAHs; $C_{28}H_{14}$ and $C_{28}H_{16}$. Molecules with higher or lower hydrogen content would not be benzenoid PAHs. In general, benzenoid PAHs are restricted to a rather small range of hydrogens and carbons.[69] The mass peaks of $C_{28}H_{14}$ and $C_{28}H_{16}$ would be separated by 2 amu, which could well be resolved by our instrument. We conclude that only one of the two $C_{28}H_x$ PAHs occurs in the flame. While the $C_{28}H_{14}$ PAHs occur with high abundance, the $C_{28}H_{16}$ peak is missing. Obviously, this PAH is not formed in the flame.

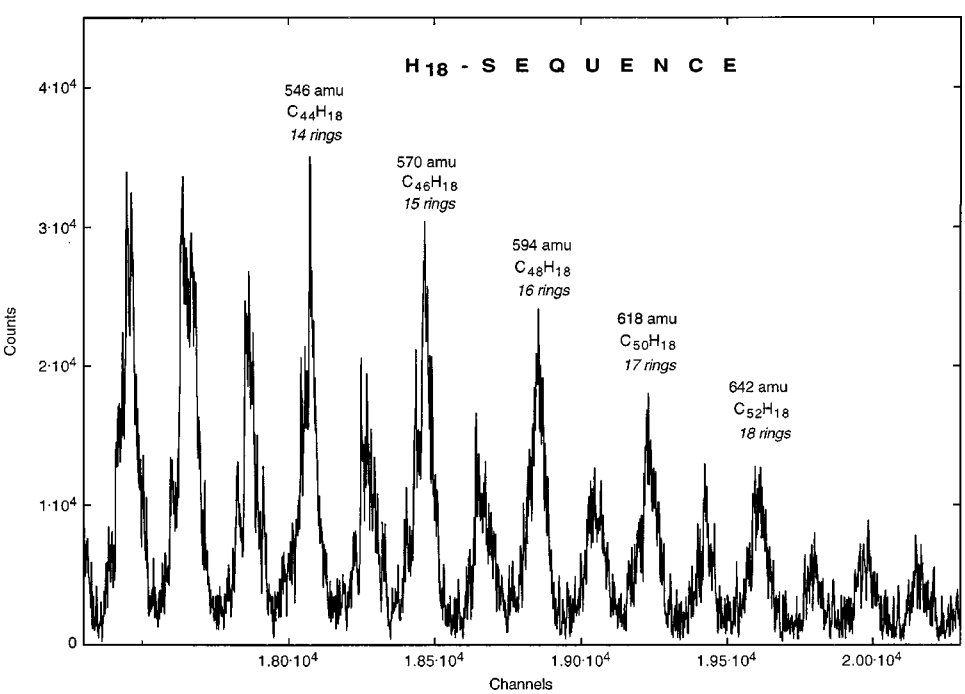

FIG. 5. Section of the mass spectrum, showing the H_{18}-sequence.

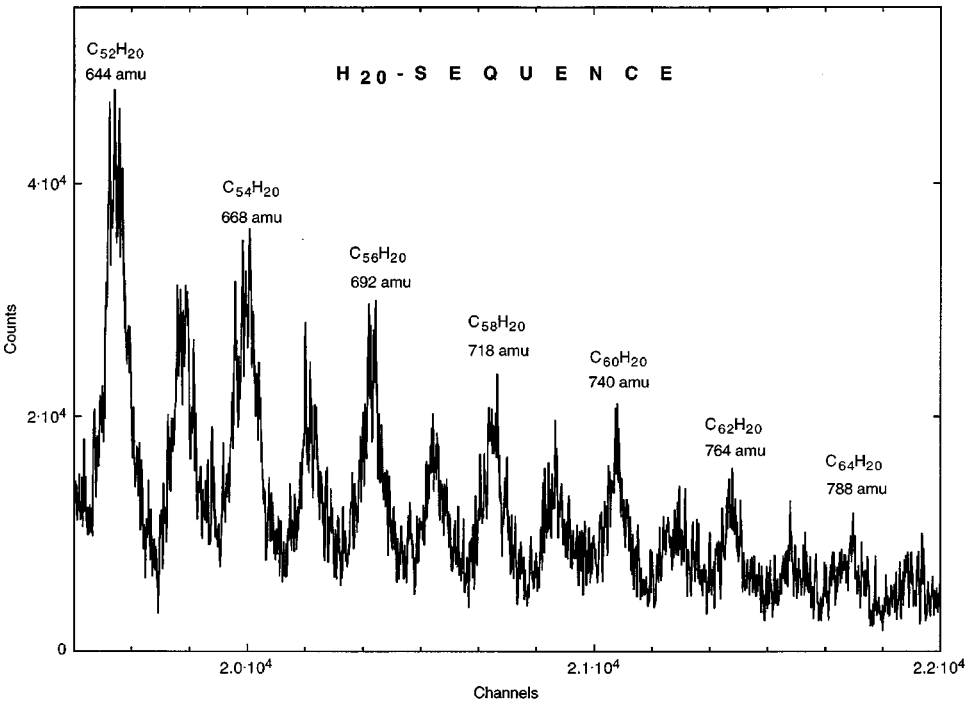

FIG. 6. Section of the mass spectrum, showing the H_{20}-sequence.

For the C_{30}-core, the possible PAHs may have the three masses 374, 376, and 378 amu, corresponding to the formulas $C_{30}H_{14}$, $C_{30}H_{16}$, and $C_{30}H_{18}$, respectively. The locations of the expected mass peaks are indicated in Fig. 7. At 374 amu we observe a strong peak and assign it to $C_{30}H_{14}$. The other two PAHs, at 376 and 378 amu however, are missing. In chemical processes these PAHs have been synthesized. For example, the molecule pyranthrene ($C_{30}H_{16}$) is a stable and well-known benzenoid compound.[73] Yet, this PAH obviously does not form in the flame.

The $C_{32}H_x$ PAH group could consist of three peaks; $C_{32}H_{14}$, $C_{32}H_{16}$, and $C_{32}H_{18}$. Again, only the one with the smallest H content appears in the mass spectrum, and the ones with higher H content are not formed in the flame. Comparing the observed mass peaks in Fig. 7 we can see that they differ by exactly 24 amu, which is due to the fact that for each possible PAH only the one with the smallest mass is formed in the flame.

Figure 8 shows another three prominent mass peaks (448, 472, and 496 amu) with the corresponding Lorentz

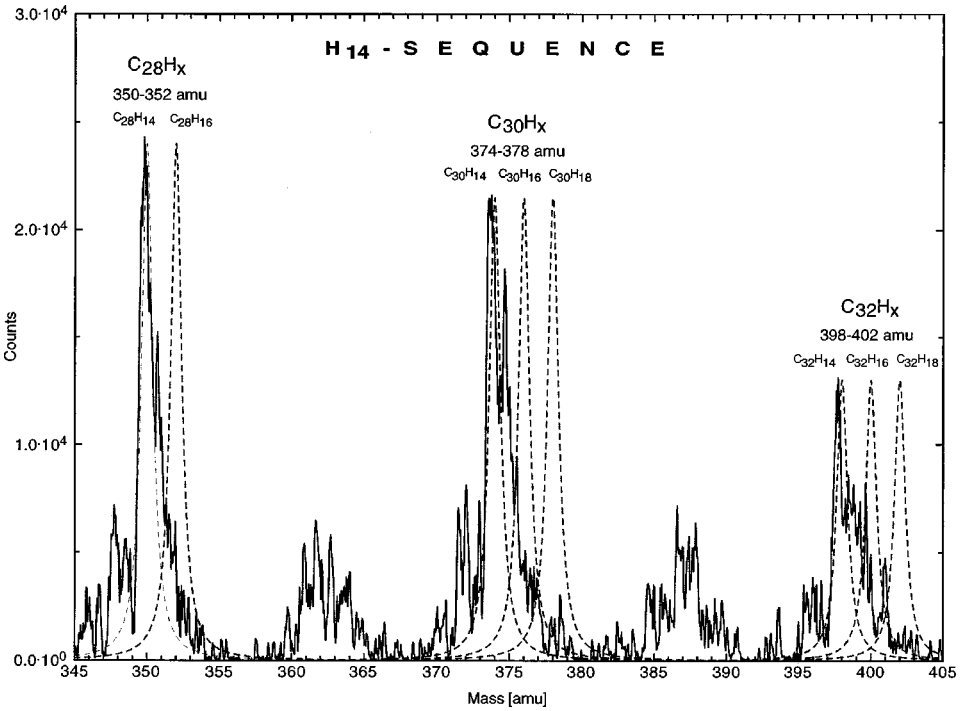

FIG. 7. Section of the mass spectrum. Peaks of PAHs, not found in the flame, are also indicated.

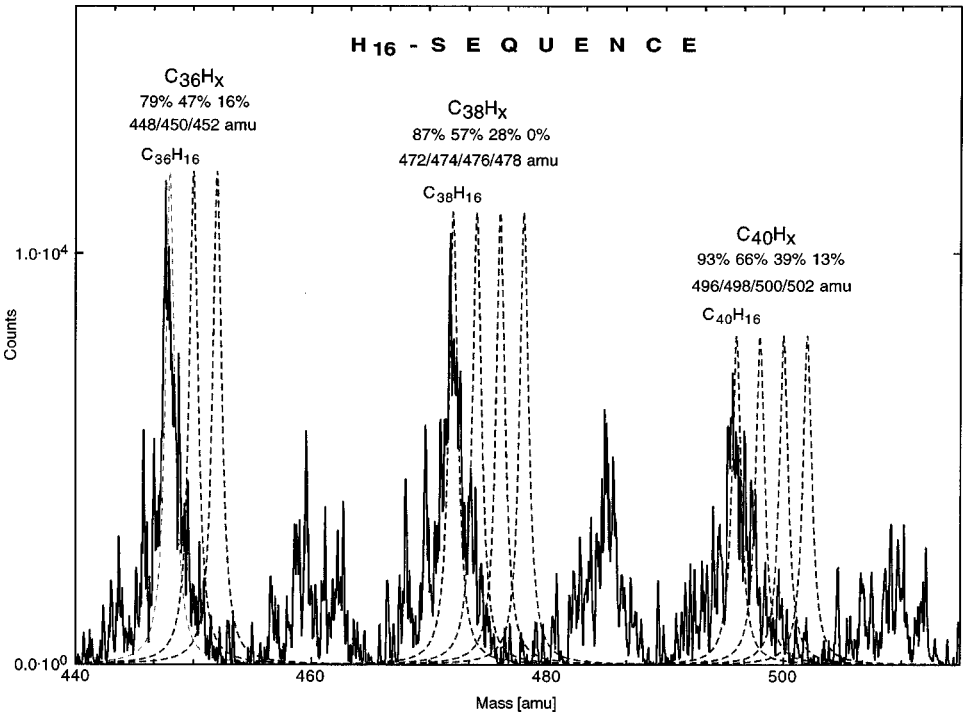

FIG. 8. Section of the mass spectrum. Peaks of PAHs, not found in the flame, are shown by Lorentz curves for $C_{36}H_x$, $C_{38}H_x$, and $C_{40}H_x$.

curves for all possible PAHs, 2 amu apart in each set. The $C_{36}H_x$ group consists of three subgroups, the $C_{38}H_x$ and $C_{40}H_x$ groups of four subgroups each. Again, we find that only the PAHs with the smallest H contents are realized in the flame, for each of the three groups. In this figure we also give the percentage of condensation of the fused rings in the PAHs. This is determined by considering the C/H ratio for different PAHs on a scale between 0% and 100%. 0% refers to the least compact (cata-condensed) PAH and 100% to the most compact (circular) PAHs. The formulas for determination of the 0% and 100% border lines were derived earlier.[69]

For the cata-condensed PAHs, the borderline is given by $N_C = 2*N_H - 6$ and for the most compact (circular) PAHs by $N_C = (1/6)*N_H^2$. The percentage values for PAHs within the border lines are determined by linear interpolation. For example, we determine for the PAHs with the C_{36} core and formulas $C_{36}H_{16}$, $C_{36}H_{18}$, and $C_{36}H_{20}$, the degrees of condensation as $D_c = 79\%$, 47%, and 16%, respectively.

The same features and tendencies can also be seen in Fig. 9 for the sequence of even-numbered peaks $C_{44}H_{18}$, $C_{46}H_{18}$, $C_{48}H_{18}$, and $C_{50}H_{18}$. Clearly, only the peaks with the

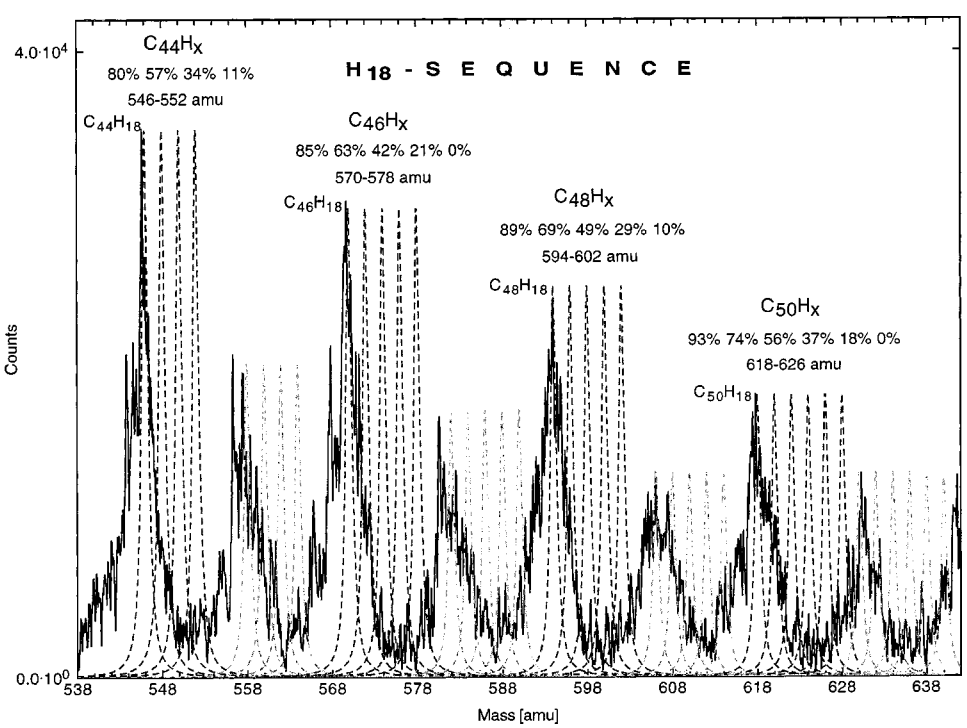

FIG. 9. Section of the mass spectrum of the H_{18}-sequence. All peaks for possible even- and odd-numbered PAH peaks are shown by Lorentz curves.

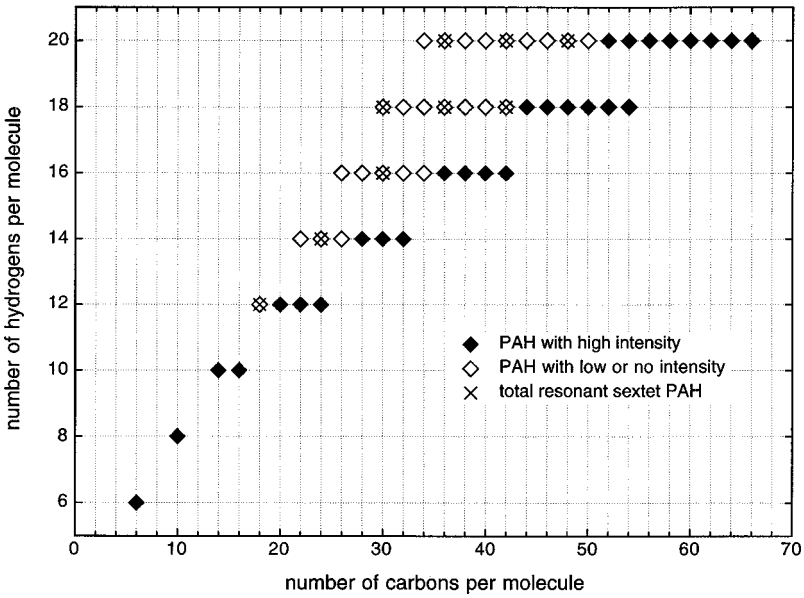

FIG. 10. All benzenoid PAHs (with up to 20 hydrogens) ordered in a H versus C diagram. PAHs found in the flame are marked with filled symbols; PAHs not found are represented by open symbols. C_xH_y PAHs having at least one isomer for which Clar's sextet rule applies are marked by a cross.

smallest H contents and the highest packing densities of hexagons are realized in the flame. In Fig. 9 we also plot Lorentz curves for the benzenoid PAHs with an odd number of carbons. Again, the most condensed species have the highest abundance. Odd-numbered PAHs give two signals in the mass spectrum separated by one mass unit. We assume that a hydrogen atom bound to the sp^3 carbon atom is lost easily upon ionization, because thereby a stable cation is formed. The result is that a mass peak appears in the spectrum with 1 amu off the Lorentz curve. We see in Fig. 9 that the mass peaks of possible PAHs, represented by the Lorentz curves, would fill the entire spectrum. Although all of them are generally stable, only the most condensed ones are formed in the flame.

Figures 7–9 display mass spectra in subsequently higher mass regions. We can see that the number of possible PAHs belonging to one C_n-core, increases with larger PAH mass. While the C_{28}-core (Fig. 7) has only two possible PAH formula units ($C_{28}H_{14}$ and $C_{28}H_{16}$), the C_{50}-core has six PAH formula units ($C_{50}H_{18}$, $C_{50}H_{20}$, $C_{50}H_{22}$, $C_{50}H_{24}$, $C_{50}H_{26}$, $C_{50}H_{28}$).

In Fig. 10 the PAHs are sorted in a C–H diagram. Filled symbols stand for PAHs having high intensity in the mass spectra; open symbols are PAHs with zero or low intensity. Horizontal lines in this figure correspond to the sequences with constant H content as given above. With increasing number of hydrogens the spread of possible PAHs becomes larger. In the H_{20}-series, for example, 17 PAH mass peaks are possible. The PAHs on a vertical line have the same number of carbon atoms. As shown in the mass spectra, only the ones with the smallest hydrogen contents are realized in the flame. The upper border line of the distribution of PAHs in Fig. 10 belongs to the cata-condensed PAHs. It is a straight line (from C_6H_6 to $C_{34}H_{20}$) with the formula given above. The most compact, peri-condensed PAHs are represented by the lower border line (from C_6H_6 to $C_{66}H_{20}$). The square-root expression for this curve has been given above.

Generally, the most stable PAHs are those containing only total resonant sextets (a set of three double bonds that are mutually permutable within the same hexagonal ring). This characteristic is called ''Clars sextet rule.'' [74] In Fig. 10 those C_xH_yPAHs that have an isomer belonging to the total resonant sextet class are marked by a cross. It is seen that none of the total resonant sextet PAHs is found in the flame.

For a given number of carbon and hydrogen, many isomeric benzenoid PAHs can be constructed. The number of isomers as given by Dias[75] are plotted in Fig. 11 as a function of the number of carbons in the PAHs. Overall, it can be seen that the number of isomers increases rapidly with PAH size, by many orders of magnitude. The PAHs found in the experiment are given by filled symbols and arranged according to their hydrogen content. The PAHs which are not formed in the flame are plotted with open symbols. The number of isomers for the various H_x sequences differ by approximately a factor of 10. Surprisingly, we find that in the flame there exist only those PAHs with a small number of isomers. For example, $C_{60}H_{20}$ has 32 isomers and is observed in the flame, whereas $C_{60}H_{22}$, $C_{60}H_{24}$, and $C_{60}H_{26}$ have 5726, 116 648, and 1 262 442 isomers, respectively, and are not observed. This result is intriguing as it shows that the number of possible structures plays a minor role in PAH formation.

In Fig. 12 we show structures arranged in a spreadsheet which can explain the observed peaks. The PAHs within each row contain the same number of H atoms. Each row ends with a zigzag-type PAH, shown in the column on the right side. A zigzag PAH does not contain any bays. The PAHs in this column can be regarded as groups of three: The groups (H_6-H_{10}, $H_{12}-H_{16}$, $H_{18}-H_{22}$) are composed of one, two, and four hexagons (in the center), with zero, one, and two surrounding shells of hexagons, respectively. This building principle is illustrated in Fig. 13.

The structures in Fig. 13 are the first nine most compact PAHs. Their formulas can be expressed by the equation $N_C = \text{integer}(N_H^2/6)$ for $N_H = 6$, 8, 10, 12, etc. These PAHs

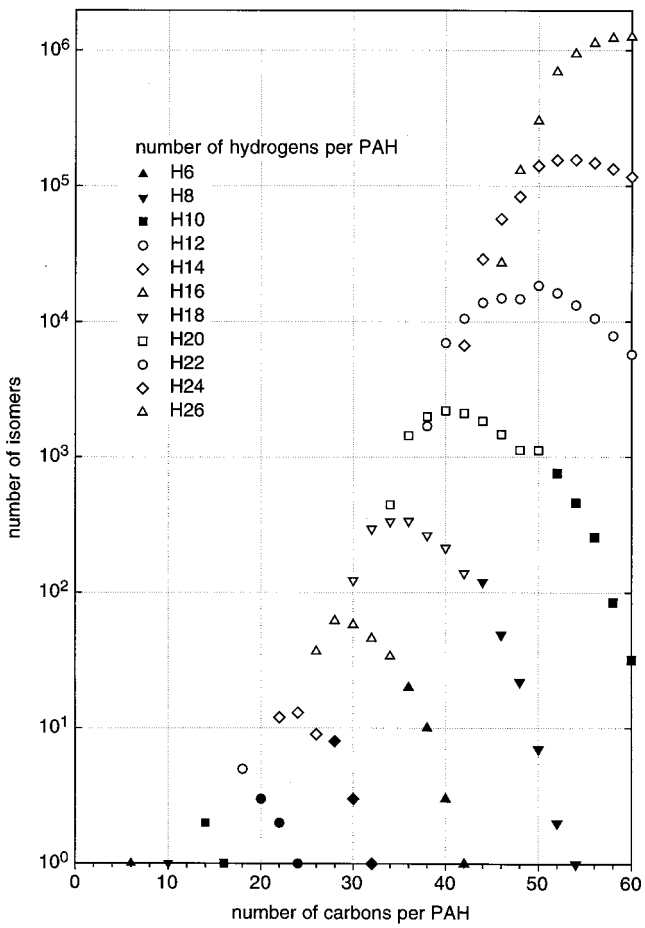

FIG. 11. The number of isomers for benzenoid PAHs as a function of number of carbons for each H sequence in a logarithmic plot. Filled symbols stand for PAHs found in the flame.

belong to three families, which we name after their first member: The benzene family, the naphthalene family, and the pyrene family. These molecules are shown in the first column in Fig. 13. The higher members of a family are obtained by arranging shells of hexagons around the core (second and third column). Following the notation given by Dias,[75] the first two higher members of the benzene family are circum(18)benzene (coronene) ($C_{24}H_{12}$) and bicircum(48)benzene ($C_{54}H_{18}$); those of the naphthalene family are circum(22)naphthalene (ovalene) ($C_{32}H_{14}$) and bicircum(56) naphthalene ($C_{66}H_{20}$); and those of the pyrene family are circum(26)pyrene ($C_{42}H_{16}$) and bicircum(64)pyrene ($C_{80}H_{22}$).

The PAHs from the naphthalene and pyrene families are less compact than those from the benzene family. Within the benzene family ($N_H=6n$), $N_H^2/6$ always produces an integer number. In the naphthalene family ($N_H=6n+2$), the division $N_H^2/6$ yields the residual 0.333 and in the pyrene family ($N_H=6n+4$) the residual 0.666 is always obtained. The most compact benzenoid PAHs are the endpoints of the constant-H sequences (last column in Fig. 12).

Each row in Fig. 12 starts on the left side with an armchair-type PAH which contains several bays and ends on the right side with a PAH without bays. In order to explain PAH growth and the predominance of low hydrogen-containing PAHs, we postulate the PAH growth mechanism shown in Fig. 14. This mechanism is an example of the Diels–Alder reaction, wherein acetylene is the dienophil and a bay region of a PAH (phenanthrene is shown as an example) is the diene. In an electrocyclic addition reaction, acetylene adds to the bay region thus forming a new, six-membered ring. This ring subsequently loses two hydrogen

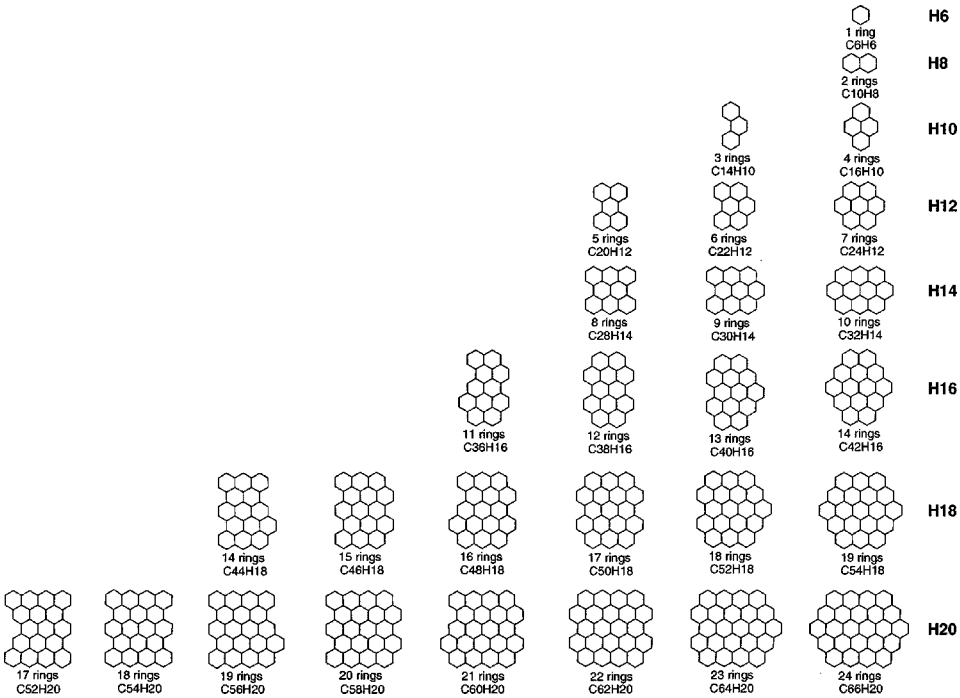

FIG. 12. PAHs found in the flame ordered in constant-H sequences. In each H sequence the PAHs are ordered as a function of the number of rings. Only one PAH for each formula unit is drawn representing all isomers. Hydrogens and π-bonds are omitted for clarity.

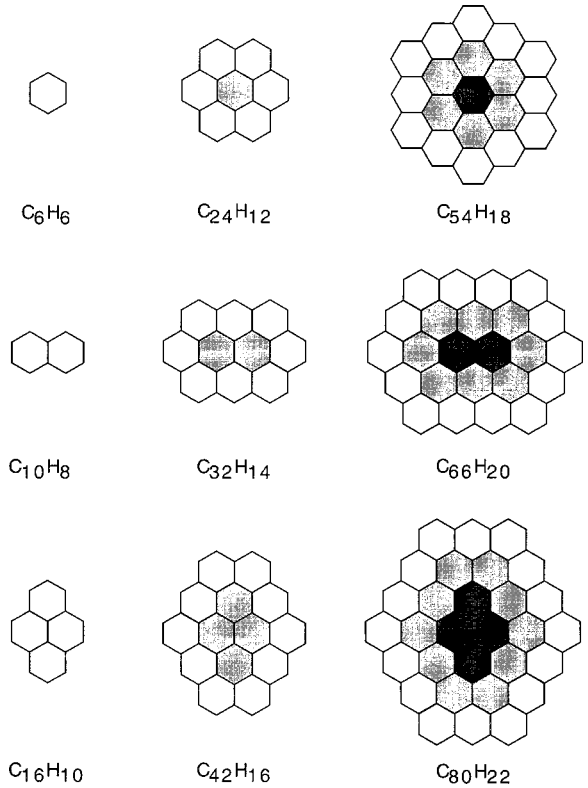

FIG. 13. The first most compact benzenoid PAHs. They can be found by drawing shells of hexagons around a benzene, naphthalene, or pyrene core, respectively.

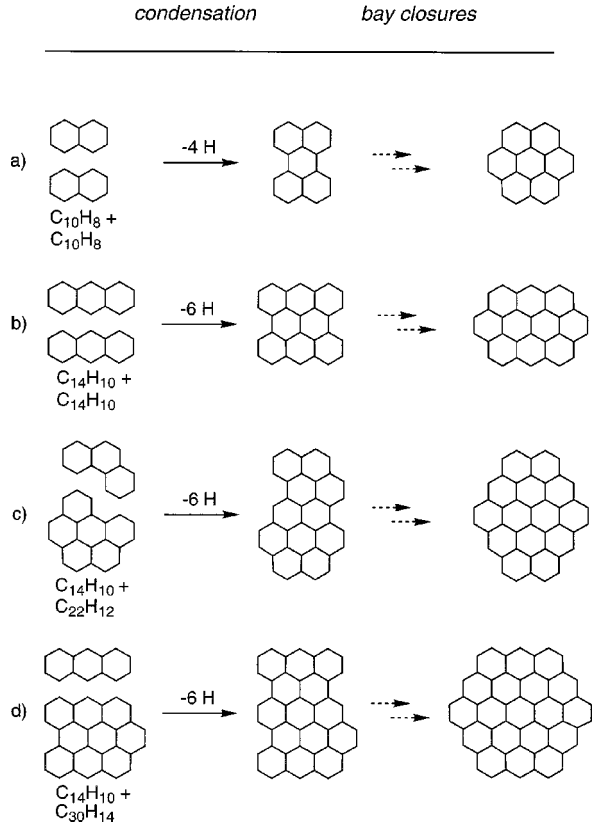

FIG. 15. Condensation reactions of small PAHs, forming the starting PAHs for the H sequences in Fig. 12. Those PAHs will then react by subsequent Diels–Alder reactions forming the most compact PAHs.

atoms and becomes aromatic. A PAH with two additional carbons and one additional ring is formed (pyrene in the example).

This reaction is not unprecedented. Bay regions of PAHs can react as dienophil, for example Benzo(ghi)perylene ($C_{22}H_{12}$, Fig. 12) reacts with maleic anhydride ($C_4H_2O_3$) to form (after decarboxylation) coronene ($C_{24}H_{12}$, Fig. 12).[74] This is the best way to prepare coronene. The reaction is often called the ''benzogenic Diels–Alder reaction.''[1] Acetylene can act as dienophil in the sense as shown in Fig. 14,[76] although this reaction has not been reported to occur with PAHs. We therefore propose that the benzogenic Diels–Alder reaction with acetylene as dienophil, together with the conventional hydrogen abstraction acetylene addition (HACA) mechanism,[55,77] is an important PAH growth process. This mechanism has the advantage over the HACA process to explain the formation of successively more compact, peri-condensed PAHs, as they are found in our spectra.

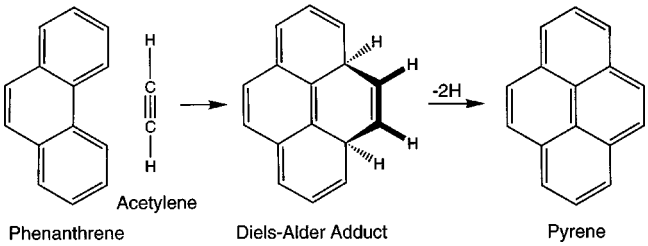

FIG. 14. The ''benzogenic Diels–Alder reaction'' with phenanthrene (as an example) and acetylene. This bay closing reaction is postulated in order to explain the observed PAH sequences with 24 amu spacing.

Once all bays of a constant-H sequence are closed, successive growth to the start of the next-higher constant-H sequence is not possible. This is because each sequence starts with a molecule of high bay content, which cannot be formed by the conventional HACA process.

We propose that the beginning of each constant-H sequence is produced by reactive coagulation of smaller PAHs. In previous experiments we have shown for $C_{20}H_{12}$ and $C_{28}H_{14}$, the first PAH of the H_{12} and H_{14} sequences,[69] that such coalescence is an important process in the flame. In height profiles from a laminar methane diffusion flame, we found that $C_{20}H_{12}$ and $C_{28}H_{14}$ are formed more rapidly than other PAHs of similar mass. Their formation could not be explained by successive growth. In Fig. 15 we illustrate schematically the reactive coagulation processes for the formation of those PAHs which are at the beginning of the H_x sequences.

There are many possible dimerization reactions due to the large number of PAH isomers. For the formation of $C_{36}H_{16}$ we list all 20 isomers with descending stability[2] (Fig. 16, row a). All possible dimers, which could coagulate in principle to the 20 isomers, are given in rows b, c, and d. For example, the PAH with structure 11a has three dimers as possible coagulation precursors.

A condition for the dimerization to occur is that both partners are abundant in the flame. This is not given for most of the dimers listed in Fig. 16. Only three cases remain: 2b, 3b, and 8b. These three cases can further be reduced to only

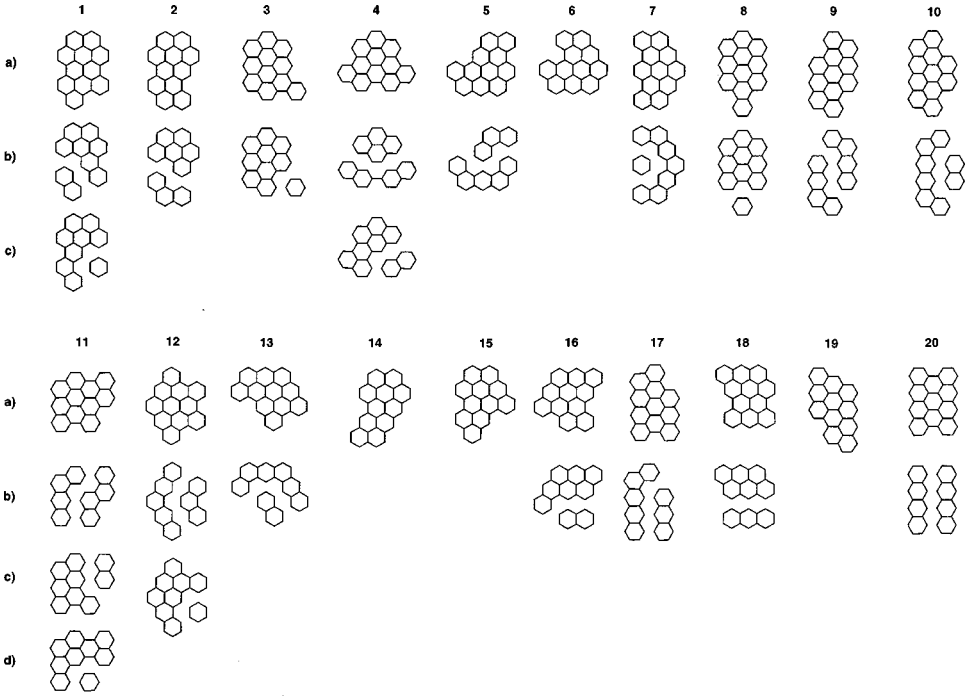

FIG. 16. The possible PAH dimerization reactions forming all 20 benzenoid $C_{36}H_{16}$ isomers.

one (2a). In order to be the first member of the H_{16} sequence (Fig. 12), the $C_{16}H_{36}$ PAH must have three closable bays. This is only the case for structure 2a. Therefore, this process is selected and plotted in Fig. 15.

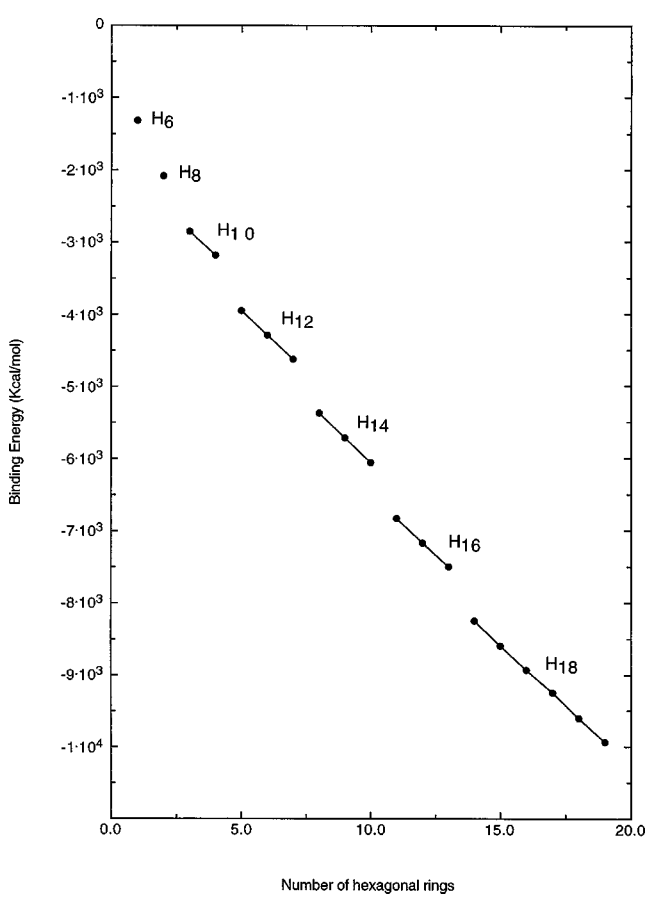

FIG. 17. Binding energy for PAHs as a function of number of hexagonal rings for the different H sequences as calculated by PM3.

In Fig. 17 we plot the binding energies (BE) calculated by PM3 for the observed PAHs, as a function of increasing number of hexagonal rings. PM3, a semiempirical, quantum chemical theory developed by Stewart,[78] is a reparametrization of AM1 (Austin model 1[79]). We see that the increase in BE (plotted on a negative scale) is uniform within each H_n sequence. There are pronounced steps in the BE plot when going from one series to the next. The BE changes by about 340 kcal/mol within one sequence, but by more than twice this value from one sequence to the next.

In Fig. 18 we plot the ''periodic formula table'' of PAHs as given by Dias.[75] The formula units are arranged according to two parameters: the number of inner carbons N_{Ic}, and the net number of disconnections among the internal edges d_s. N_{Ic} is equivalent to the number of third-degree vertices, bounded by three hexagonal rings. Second-degree vertices are caused by two hexagons. The number of second-degree vertices is equal to the number of carbons in the PAH. The number of third-degree vertices is equal to the number of carbons minus the number of hydrogens. In order to compare formula units at different locations in the table, shift coordinates are defined as $(\Delta d_s, \Delta N_{\mathrm{Ic}}/2)$. Benzenoids having the same number of rings have shift coordinates of (2, 1). The parameters d_s, N_{Ic}, and N_r (number of rings) are related by the equation $d_s + N_{\mathrm{Ic}} - N_r = -2$. In Fig. 18 we give the number of rings together with the formula units. Examples illustrating the way to determine the parameter d_s are given in Fig. 19.

The table in Fig. 18 follows a triad principle. In each row the successive formulas are incremented by C_4H_2 and in each column by C_6H_2. One can go either horizontally along a row, vertically in a column, or diagonally, and the middle formula of a triad is always the arithmetic mean of the other two. There are various other trends in the table.[75] Average values of the highest occupied molecular orbital (HOMO)

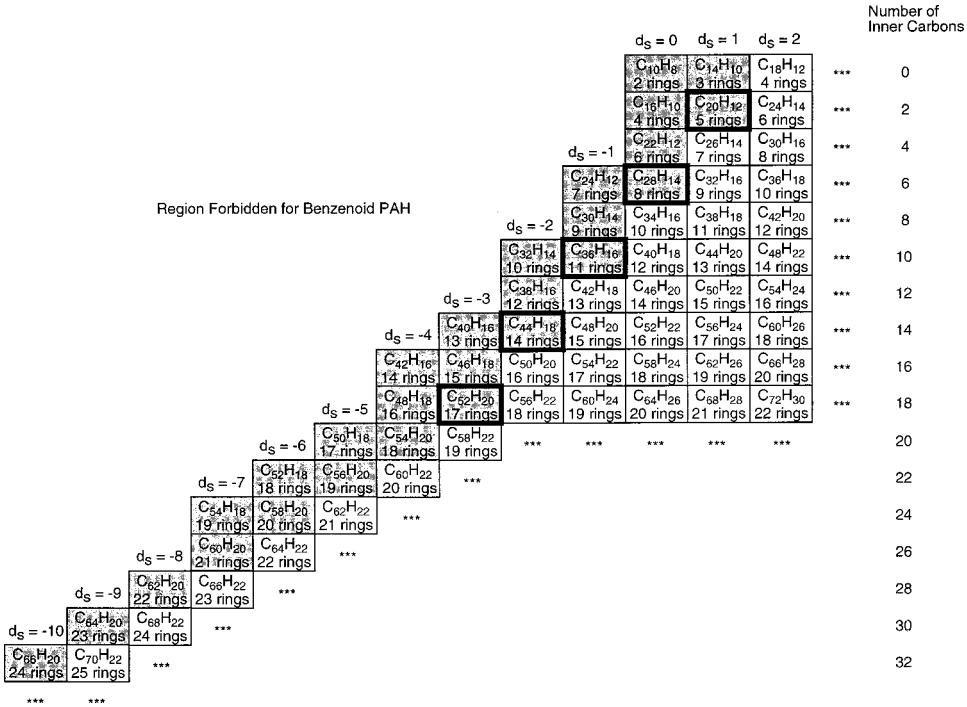

FIG. 18. Formula periodic table of the benzenoid PAHs. The PAHs found in the flame are shaded in gray. The first PAH for the observed H sequences are framed with bold lines. They can be connected by a straight line within the periodic system.

decrease in a row from left to right and in a column from top to bottom. The magnitude of the HOMO is a measure for a molecule to retain its valence electrons. Average boiling points increase in each row from left to right and in each column from top to bottom. Isomer numbers increase from left to right in each row and from top to bottom in each column.

There are three main types of benzenoid PAHs: (i) cata-condensed, (ii) strictly peri-condensed, and (iii) peri-condensed with cata-condensed appendages. Cata-condensed PAHs have no internal third-degree vertices. They appear at positive values of d_s in the PAH table. A strictly condensed benzenoid PAH has all its internal third-degree vertices mutually connected, i.e., it has no cata-condensed appendages. These PAHs have large negative d_s values. The formula units of peri-condensed PAHs with large cata-condensed appendages may appear at positive d_s values even though the peri-condensed part has compact structure. It follows that only the strictly peri-condensed PAHs (with no appendages) are located at the borderline on the left side in the PAH table.

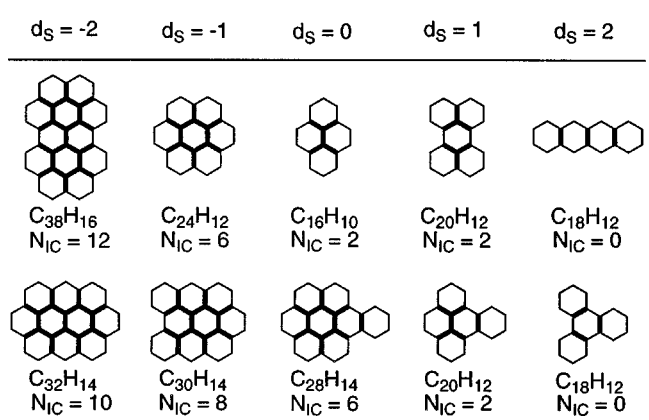

FIG. 19. Examples illustrating the net number of disconnections among the internal edges (d_s) and the number of inner carbons (N_{Ic}) for benzenoid PAHs. The internal edges are drawn in bold.

Benzenoid isomers are called isovalent since the number of second- and third-degree vertices remain unchanged in going from one isomer to another. For example, benzo(a)pyrene and perylene are isovalent $C_{20}H_{12}$ isomers. Therefore, the PAHs can well be arranged in a two-dimensional array of formula units by using d_s and N_{Ic} as coordinate axes. The table separates cata-condensed from peri-condensed PAHs. Cata-condensed benzenoids have $N_{Ic}=0$, $d_s \geqslant 0$, and are located in the first row of the table. The left-hand edge in the table contains formulas belonging to the highest-condensed PAHs.

The formula units for the PAHs which we find in the flame are shaded in gray. In addition, we circumscribe those formulas with thick lines, which are at the beginning of the observed sequences: $C_{20}H_{12}$, $C_{28}H_{14}$, $C_{36}H_{16}$, $C_{44}H_{18}$, and $C_{52}H_{20}$ (see Figs. 2–9). These PAHs are arranged in a repetitive, ordered way in the periodic PAH system. They have the same shift coordinates $(-1, -2)$. This means that one moves one formula to the left and two formulas down to obtain the starting member of the next PAH sequence. The bay closure processes are described by shift coordinates $(-1, -1)$.

We obtain the following general picture: PAH growth cannot entirely be explained by an HACA mechanism. This mechanism assumes a random formation of new rings at the precursor PAH by reaction of two C_2H_2 with two neighboring sites. It describes well the growth of the smallest PAHs, $C_{10}H_8$ and $C_{14}H_{10}$. These PAHs cannot be formed by bay closure. However, once $C_{14}H_{10}$ has formed, it can grow to $C_{16}H_{10}$ by bay closure. Within each sequence, such a bay closure reaction leads to the formation of the next larger PAH. This comes to an end when the most condensed PAH, with all bays closed, has formed. The next larger PAH is formed by a coagulation mechanism. Our observations lead

to an ordered arrangement of PAHs in methane flames within a formula periodic system which is based on geometric considerations of PAH networks.

ACKNOWLEDGMENTS

The support for this work by M. Campagna, ABB Alstom Power Ltd., is gratefully acknowledged. We thank H. C. Siegmann for his continuous encouragement and many stimulating discussions.

[1] A. Bjorseth and T. Ramdahl, *Handbook of Polycyclic Aromatic Hydrocarbons* (Dekker, New York, 1985).
[2] J. R. Dias, *Handbook of Polycyclic Hydrocarbons* (Elsevier, Amsterdam, 1987).
[3] G. Grimmer, *Environmental Carcinogens: Polycyclic Aromatic Hydrocarbons: Chemistry, Occurrence, Biochemistry, Carcinogenity* (CRC Press, Boca Raton, FL, 1983).
[4] K. E. Thrane and A. Mikalsen, Atmos. Environ. **15**, 909 (1981).
[5] J. O. Allen, K. M. Dookeran, K. A. Smith, A. F. Sarofim, K. Taghizadeh, and A. L. Lafleur, Environ. Sci. Technol. **30**, 1023 (1996).
[6] C. Venkataraman and S. K. Friedlander, Environ. Sci. Technol. **28**, 563 (1994).
[7] *Monographs on the Evaluation of the Carcinogenic Risk of Chemicals to Humans*, Vol. 46 [International Agency for Research on Cancer (IARC), Lyon, France, 1989].
[8] R. N. Westerholm, J. Almen, H. Li, J. U. Rannug, K. E. Egeback, and K. Gragg, Environ. Sci. Technol. **25**, 332 (1991).
[9] W. F. Rogge, L. M. Hildemann, M. A. Mazurek, G. R. Cass, and B. R. T. Simoneit, Environ. Sci. Technol. **27**, 636 (1993).
[10] R. Hammerle, D. Schuetzle, and W. Adams, Environ. Health Perspect. **102**, 25 (1994).
[11] J. H. Johnson, S. T. Bagley, L. D. Gratz, and D. G. Leddy, Soc. Automot. Eng. Trans. **103**, 210 (1994).
[12] D. H. Lowenthal, B. Zielinska, J. C. Chow, J. G. Watson, M. Gautam, D. H. Ferguson, G. R. Neuroth, and K. D. Stevens, Atmos. Environ. **28**, 731 (1994).
[13] L. D. Gratz, S. T. Bagley, D. G. Leddy, G. M. Pataky, K. J. Baumgard and J. H. Johnson, Abstr. Pap. Am. Chem. Soc. **204**, 9-PETR (1992).
[14] T. Nielsen, Atmos. Environ. **30**, 3481 (1996).
[15] D. T. Kaschani, Staub-Reinhalt. Luft **43**, 3 (1983).
[16] R. M. Kamens and D. L. Coe, Environ. Sci. Technol. **31**, 4 (1997).
[17] T. Spitzer and S. Kuwatsuka, Environ. Pollut. **62**, 63 (1989).
[18] S. V. Pisupati and R. S. Wasco, Abstr. Pap. Am. Chem. Soc. **216**, 049-ENVR (1998).
[19] P. Masclet, M. A. Bresson, and G. Mouvier, Fuel **66**, 7 (1987).
[20] L. A. Gundel, V. C. Lee, K. R. R. Mahanama, and R. K. Stevens, Atmos. Environ. **29**, 1719 (1995).
[21] G. Loefroth, Chemosphere **7**, 791 (1978).
[22] T. Ramdahl, Nature (London) **306**, 580 (1983).
[23] A. Atal, Y. A. Levendis, J. Carlson, Y. Dunayevskiy, and P. Vouros, Combust. Flame **110**, 17 (1997).
[24] I. Alfheim and T. Ramdahl, Environ. Mutagen. **6**, 121 (1984).
[25] T. Panagiotou, Y. A. Levendis, J. Carlson, Y. M. Dunayevskiy, and P. Vouros, Combust. Sci. Technol. **116**, 39 (1996).
[26] S. Senkan and M. Castaldi, Combust. Flame **107**, 10 (1996).
[27] A. Ciajolo, A. D'Anna, and R. Barbella, Combust. Sci. Technol. **100**, 271 (1994).
[28] H. Hepp, K. Siegmann, and K. Sattler, Chem. Phys. Lett. **233**, 16 (1995).
[29] A. S. Feitelberg, J. P. Longwell, and A. F. Sarofim, Combust. Flame **92**, 13 (1993).
[30] H. Wang and M. Frenklach, Combust. Flame **110**, 49 (1997).
[31] N. M. Marinov, W. J. Pitz, C. K. Westbrook, M. J. Castaldi, and S. M. Senkan, Combust. Sci. Technol. **116**, 77 (1996).
[32] J. A. Marr, L. M. Giovane, J. P. Longwell, J. B. Howard, and A. L. Lafleur, Combust. Sci. Technol. **101**, 301 (1994).
[33] S. Stein and A. Fahr, J. Phys. Chem. **89**, 3714 (1985).
[34] C. J. Pope and J. B. Howard, Aerosol. Sci. Technol. **27**, 22 (1997).
[35] M. Ikegami, Y. Yoshihara, and X. H. Li, B. JSME **29**, 4256 (1986).
[36] R. I. Kaiser, Y. T. Lee, H. F. Bettinger, P. R. von Schleyer, P. R. Schreiner, and H. F. Schaefer, Abstr. Pap. Am. Chem. Soc. **215**, 303-PHYS (1998).
[37] J. H. Miller, Abstr. Pap. Am. Chem. Soc. **202**, 109-FUEL (1991).
[38] K. Sakaguchi and S. Fukutani, Bull. Chem. Soc. Jpn. **65**, 5 (1992).
[39] J. Ahrens, R. Kovacs, and E. A. Shafranovskii, Ber. Bunsenges. Phys. Chem. **98**, 265 (1994).
[40] C. S. McEnally and L. D. Pfefferle, Combust. Sci. Technol. **116–117**, 183 (1996).
[41] K. Siegmann, H. Burtscher, and H. Hepp, J. Aerosol Sci. **24**, 373 (1993).
[42] R. A. Dobbins, R. A. Fletcher, and H.-C. Chang, Anal. Chem. **70**, 2745 (1998).
[43] A. L. Lafleur, K. Taghizadeh, J. B. Howard, J. F. Anacleto, and M. A. Quilliam, J. Am. Soc. Mass Spectr. **7**, 276 (1996).
[44] J. T. McKinnon, E. Meyer, and J. B. Howard, Combust. Flame **105**, 6 (1996).
[45] T. Visser, M. Sarobe, L. W. Jenneskens, and J. W. Wesseling, Fuel **77**, 8 (1998).
[46] H. Burtscher and H. C. Siegmann, Combust. Sci. Technol. **101**, 6 (1994).
[47] Th. Henning and F. Salama, Science **282**, 2204 (1998).
[48] D. M. Hudgins and L. J. Allamandola, Astrophys. J. **516**, L41 (1999).
[49] N. Ladommatos, P. Rubenstein, K. Harrison, Z. Xiao, and H. Zhao, J. I. Energy **70**, 84 (1997).
[50] J. M. Smedley, A. Williams, and K. D. Bartle, Combust. Flame **91**, 71 (1992).
[51] C. S. McEnally and L. D. Pfefferle, Combust. Sci. Technol. **128**, 257 (1997).
[52] M. J. Castaldi, A. M. Vincitore, and S. M. Senkan, Combust. Sci. Technol. **107**, 19 (1995).
[53] A. M. Vincitore and S. M. Senkan, Combust. Flame **114**, 8 (1998).
[54] A. M. Vincitore and S. M. Senkan, Combust. Sci. Technol. **130**, 14 (1997).
[55] P. Weilmunster, A. Keller, and K. H. Homann, Combust. Flame **116**, 22 (1999).
[56] A. L. Lafleur, J. B. Howard, E. Plummer, K. Taghizadeh, A. Necula, L. T. Scott, and K. C. Swallow, Polycycl. Aromat. Compd. **12**, 223 (1998).
[57] N. M. Marinov, M. J. Castaldi, C. F. Melius, and W. Tsang, Combust. Sci. Technol. **128**, 48 (1997).
[58] Z. A. Mansurov, G. O. Turesheva, V. I. Pesterev, V. T. Popov, and A. A. Merkulov, Petrol. Chem. **31**, 5 (1991).
[59] N. M. Marinov, W. J. Pitz, C. K. Westbrook, A. M. Vincitore, M. J. Castaldi, S. M. Senkan, and C. F. Melius, Combust. Flame **114**, 22 (1998).
[60] M. J. Castaldi and S. M. Senkan, Combust. Sci. Technol. **116**, 167 (1996).
[61] J. A. Cole, J. D. Bittner, J. P. Longwell, and J. B. Howard, Combust. Flame **56**, 20 (1984).
[62] S. T. Kolaczkowski, Chem. Eng. Res. Des. **73**, 168 (1995).
[63] K. Eguchi and H. Arai, Catal. Today **29**, 379 (1996).
[64] S. R. Vatcha, Energy Convers. Manage. **38**, 1327 (1997).
[65] A. L. Lafleur, J. B. Howard, K. Taghizadeh, E. F. Plummer, L. T. Scott, A. Necula, and K. C. Swallow, J. Phys. Chem. **100**, 8 (1996).
[66] M. Kasper and K. Siegmann, Combust. Sci. Technol. **140**, 333 (1998).
[67] M. Kasper, K. Siegmann, and K. Sattler, J. Aerosol Sci. **8**, 1569 (1997).
[68] M. Kasper, K. Sattler, K. Siegmann, and U. Matter, J. Aerosol Sci. **29**, 717 (1998).
[69] K. Siegmann, H. Hepp, and K. Sattler, Combust. Sci. Technol. **109**, 165 (1995).
[70] K. Siegmann, H. Hepp, and K. Sattler, Surf. Rev. Lett. **3**, 5 (1996).
[71] H. Hepp and K. Siegmann, Combust. Flame **115**, 275 (1998).
[72] M. Kasper, K. Sattler, K. Siegmann, U. Matter, and H. C. Siegmann, J. Aerosol Sci. **30**, 217 (1999).
[73] H. Inokuchi, S. Shiba, T. Handa, and H. Akamatu, Bull. Chem. Soc. Jpn. **25**, 299 (1952).
[74] E. Clar, *Polycyclic Hydrocarbons* (Academic, London and New York, 1964).
[75] J. R. Dias, Polycycl. Aromat. Comp. **4**, 87 (1994).
[76] J. March, *Advanced Organic Chemistry* (Wiley, New York, 1992).
[77] J. T. McKinnon and J. B. Howard, Combust. Sci. Technol. **74**, 175 (1990).
[78] J. J. P. Stewart, J. Comput. Chem. **10**, 209 (1989).
[79] M. J. S. Dewar, E. G. Zoebisch, E. F. Healy, and J. J. P. Stewart, J. Am. Chem. Soc. **107**, 3902 (1985).